Research Article

Numerical Study of Acoustic-Electric Signal Conversion for GIS Discharge Detection and Structure Optimization for pMUT

Wen-Rong Si [ID],[1] Ying-Ying Zhao,[1] Zheng-Yong Hu,[1] Chen-Zhao Fu,[1] Bo Wang,[2] and Jian Yang [ID][2]

[1]State Grid Shanghai Electrical Power Research Institute, Shanghai 200437, China
[2]MOE Key Laboratory of Thermo-Fluid Science and Engineering, Xi'an Jiaotong University, Xi'an 710049, China

Correspondence should be addressed to Jian Yang; yangjian81@mail.xjtu.edu.cn

With the development of microelectromechanical technology, the piezoelectric micromechanical ultrasonic transducer (pMUT) for ultrasonic detection of gas-insulated switchgear (GIS) breakdown discharge has become possible. In this article, the ultrasonic-solid-pMUT coupling simulation model was established to investigate the propagation process of ultrasonic waves in GIS enclosure and the conversion between ultrasonic and electric signals through pMUT. The output electric signals for the unsimplified top electrode and simplified top electrode model were compared, and the structure of receiving pMUT was optimized according to the main ultrasonic frequency range of GIS breakdown discharge and the key performance parameters of pMUT. First, it is found that the simulation results of the ultrasonic-solid-pMUT coupling model are reliable, and the frequency of the output electric signal of receiving pMUT is consistent with the input signal, while the amplitude of output signal attenuates greatly. Second, simplifying the top electrode of pMUT may lead to relatively large errors in simulation results. The output response of simplified pMUT is obviously weakened, and the inherent frequency is higher. Furthermore, it is noted that the pMUT inherent frequency (f_0) is inversely proportional to the radius (R) of the piezoelectric layer and directly proportional to the substrate thickness (d_{si}). When the coverage rate of the top electrode is between 30% and 80%, the pMUT effective electromechanical coupling coefficient (K_{eff}^2) is high and has a maximum value. Finally, it is indicated that the pMUT with the optimum structure is suitable for the detection of GIS breakdown discharge ultrasonic signals, and the K_{eff}^2 can be improved by 106.7%.

1. Introduction

Electric insulation is a key problem in the power system. The accumulation of long-term partial discharge (PD) of insulation media will eventually lead to the electrical breakdown of the entire insulation system, which will cause serious failures. Finding equipment discharge problems as soon as possible through the breakdown testing or real-time monitoring can effectively improve the system reliability and reduce the operation cost [1–3]. Gas-insulated switchgear (GIS) is a widely used high-voltage sealed switchgear in the current power system. Because GIS is a large fully enclosed device and its internal structure is complicated, the problem of insulation failure and discharge detection of GIS has been receiving great attentions

[4, 5]. In recent years, the ultrasonic detecting method has been gradually mentioned for the discharge detection of GIS, and the common ultrasonic sensors used in engineering are wired piezoelectric sensors. The basic detection mechanism is to use a piezoelectric ceramic or crystal with the piezoelectric effect to convert the high-frequency acoustic signal generated by the breakdown discharge in the GIS into an electrical signal, which is then used to locate the discharge point by comparing and processing the electrical signal output from multiple sensor terminals [6, 7]. However, this method requires a certain number of ultrasonic sensors to be arranged regularly on the surface of GIS enclosure. Since the GIS is large and complex, when multiple sensors are arranged, it is difficult to arrange wires or even the wires cannot be arranged. When arranging few

sensors, it may not guarantee the effective detection of weak signals or distortion-free detection of high-intensity signals [8].

With the continuous improvement of electromechanical system (MEMS) technology and the continuous progress of wafer level material growth technology, it is possible to use the piezoelectric micromechanical ultrasonic transducer (pMUT) for nondestructive discharge detection of GIS. The advantages of pMUT, such as miniaturization, wireless transmission, and high efficiency of acoustic-electrical conversion, are expected to solve the problems of low sensitivity and wiring difficulties of traditional ultrasonic sensors in detecting GIS breakdown discharge [9, 10]. Compared with traditional piezoelectric sensors, the basic acoustic-electrical conversion mechanism of pMUT has not changed, but the vibration mode of the piezoelectric film has changed, and the coupling of voltage, deformation, and sound waves is still realized through the piezoelectric effect of the piezoelectric material. As a result, the material of the piezoelectric layer is an important factor affecting pMUT performance. In addition, the element size, materials, and integration process of the piezoelectric layer, elastic support layer, and electrode layer will further affect the mechanical properties of pMUT, which will influence its multiple response performances [11]. Therefore, it is important to design sensors with special structures to meet specific performance requirements for pMUT applications. Although experiments can effectively verify the sensor performance, while at the design stage, the empirical formula and the equivalent circuit model are often used for the calculations, which are complex and not so accurate, and the influence of multiphysical fields cannot be well solved.

In recent years, many researchers have designed pMUT and analyzed its performance based on the numerical simulation method. Liu et al. [12] established a finite element model of the pMUT array based on the AlN film and simulated the resonant frequency, modal shape, electric impedance, and sound field under water and air loading, respectively. The deviation between the simulation results of the resonant frequency and actual measurement was only 1/3 of the deviation between the results with the analysis method and actual measurement, and the simulation results of electric impedance were consistent with the measurement values. This numerical model is reliable to predict electric and acoustic performances, which is useful to optimize pMUT structures. Wang et al. [13] proposed a piston diaphragm (PD) pMUT with the improved structure. The geometrical parameters of two different piston diaphragms of the PD-pMUT were numerically studied and optimized by using COMSOL software. Their results showed that the pMUT after structure improvement had better sound transmission performance and high-frequency bandwidth, which would provide a reference for structure improvement of pMUT. An air-pMUT coupling numerical model was established by Massimino et al. [14]. In this coupling model, the electromechanical coupling, the thermal-acoustic-structure interaction of pMUT, and the thermal-acoustic-pressure interaction during acoustic waves propagation in

the air were considered. The two-dimensional and three-dimensional computational results showed that the acoustic and mechanical responses simulated by the finite element method were in good agreement with the experimental results. This research is meaningful to guide designers to simplify the computational model because, at present, the computational cost for three-dimensional multiphysical field coupling simulations is still high. Liu et al. [15] designed a square pMUT with an outer frame electrode based on numerical simulations. They found that the square pMUT had better performance in receiving ultrasonic signals than the circle pMUT with top electrode arranged in the center, which was also confirmed by the experiments. Therefore, the finite element simulation should be an effective and convenient way for the structural design and performance analysis of pMUT. However, based on previous application fields of pMUT, the current research is still mainly focused on the electromechanical performance for a single sensor or array or their sound transmission performance in the fluid. Almost no studies were reported on ultrasonic-solid-pMUT coupling for ultrasonic signal detection of GIS breakdown discharge, and the finite element simulation model for ultrasonic-solid-pMUT coupling has not been established yet. In fact, the solid thickness measurement experiments by Xing et al. [16] showed that pMUT using piezoelectric ceramics (PZT) membranes was a promising ultrasonic-solid-state sensing and detection equipment. In addition, for the numerical simulation of pMUT, the errors caused by the model simplification and boundary settings of electrode have also not been systematically studied in the existing literatures. For example, Sammoura et al. [17] established a dual piezoelectric layer pMUT finite element simulation model, where the actual thickness of the electrode was ignored, and the piezoelectric layer boundary was used for the simulations. The errors caused by such simplifications were not discussed, which was directly ignored in the literature.

Therefore, in view of the current lack of simulation research of GIS breakdown discharge detection with pMUT and the low accuracy of pMUT design methods with the empirical formula and equivalent circuit model, in this article, a finite element simulation model of ultrasonic-solid-pMUT coupling that takes into account the acoustic transmission and the acoustic-electrical conversion process at the same time was established. Then, the conversion process between GIS breakdown discharge ultrasonic signals and pMUT electric signals was numerically studied, and the acoustic electromechanical performance of pMUT was also analyzed. In addition, the simulation errors caused by the electrode simplification were discussed by comparing the simulation results obtained from the unsimplified top electrode and simplified top electrode model. Finally, the pMUT structure was optimized by numerical simulations according to the main ultrasonic frequency range of GIS breakdown discharge and key performance parameters of pMUT, and a suitable pMUT structure was found for GIS discharge detection. This study would be meaningful for understanding the ultrasonic-solid-pMUT multiphysical field coupling transfer process and pMUT structure design for GIS breakdown discharge detection.

2. Physical Model and Computational Methods

2.1. Physical Model and Geometric Parameters. In order to detect the ultrasonic signal of breakdown discharge in the GIS, the piezoelectric sensors are required to be arranged on the outer surface of the GIS enclosure. In the present article, a coupling physical model of ultrasonic-solid-pMUT is established to analyze the output electric signals generated by the deformation of receiving pMUT, which is caused by the ultrasonic wave, as shown in Figure 1. In the simulation, the ultrasonic signal is generated through voltage excitation of emitting pMUT, which is placed on the inner surface of the GIS enclosure. The piezoelectric layer of emitting pMUT expands and shrinks due to the inverse piezoelectric effect, then bends and deforms under the binding of the elastic layer, and vibrates to emit acoustic waves. When ultrasonic waves transmit through GIS enclosure and reach the receiving pMUT arranged on the outer wall of the enclosure, the piezoelectric layer of receiving pMUT vibrates and generates induced charges due to the positive piezoelectric effect, and the electrodes output electric signals at the same time. In the present work, a two-dimensional axisymmetric model is established to study the acoustic-electric signal conversion process and a three-dimensional model is established to study the pMUT response characteristics. The circular pMUT thick film (lead zirconate titanate) is selected as the acoustic emitter and receiver. Its physical model and typical geometric parameters are shown in Figure 1 and Table 1, respectively. Since the bonding layer (epoxy adhesive) between the electrode and substrate is thin (less than $2\,\mu$m) and its Young's modulus is much smaller than that of substrate (Si), the bonding layer is neglected in the numerical model. The materials and typical physical parameters for each component of pMUT are presented in Table 2 [18, 19].

Among them, the relative permittivity of the piezoelectric layers is anisotropic, which is formulated as in the following equation [18]:

$$[\varepsilon_{\mathrm{rS1}}] = \begin{bmatrix} 762.5 & 0 & 0 \\ 0 & 762.5 & 0 \\ 0 & 0 & 663.2 \end{bmatrix},$$
$$[\varepsilon_{\mathrm{rS2}}] = \begin{bmatrix} 1704.4 & 0 & 0 \\ 0 & 1704.4 & 0 \\ 0 & 0 & 1433.6 \end{bmatrix}. \tag{1}$$

2.2. Governing Equations and Computational Methods. In the present study, the piezoelectric constitutive equations in the form of stress-charge are used to describe the relationship between stress, strain, electric field, and electric displacement of piezoelectric materials, as shown in the following equation [20]:

$$\begin{cases} S = c_{\mathrm{E}}\varepsilon - e^{\mathrm{T}}\vec{E}, \\ \vec{D} = e\varepsilon + \varepsilon_0 \varepsilon_{\mathrm{rS}}\vec{E}, \end{cases} \tag{2}$$
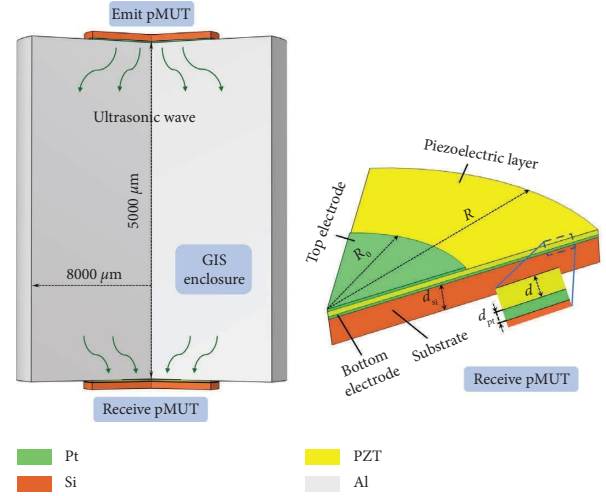

FIGURE 1: Physical model and geometric dimensions for ultrasonic-solid-pMUT coupling simulation.

TABLE 1: Typical geometric parameters for circular pMUT.

Parameters	Symbols	Values (μm)
Top electrode radius	R_0	500
Piezoelectric layer and substrate radius	R	1000
Top and bottom electrode thickness	d_{pt}	10
Piezoelectric layer thickness	d	20
Substrate thickness	d_{si}	100

where S is the stress, Pa; c_E is the Voigt elastic matrix for anisotropic materials; ε is the strain; e^T is the piezoelectric stress constant; $\vec{D}$ is the electric displacement, C/m^2; ε_0 is the initial prestrain; ε_{rS} is the relative permittivity; and $\vec{E}$ is the electric field strength, N/C.

The piezoelectric equations consist of momentum equation and electrostatic charge conservation equation. The momentum equation is based on Newton's second law equilibrium equation of solid mechanics, and the stress-charge correlation of the piezoelectric material is formulated with elastic and coupling matrices. The equations are as follows:

$$\begin{cases} \rho\dfrac{\partial^2 \vec{u}}{\partial t^2} = \nabla \cdot S, \\[4pt] \nabla \cdot \vec{D} = \rho_v, \\[4pt] S = \vec{C}: \varepsilon - \vec{E} \cdot e, \\[4pt] \vec{C} = \vec{C}([c_{\mathrm{E}}]), e = e([e_{\mathrm{ES}}]), \\[4pt] \varepsilon = \dfrac{1}{2}\left[(\nabla\vec{u})^{\mathrm{T}} + \nabla\vec{u}\right], \end{cases} \tag{3}$$

where ρ is the density, kg/m^3; $\vec{u}$ is the structural displacement vector, m; t is the time, s; ρ_v is the volume electric charge density, C/m^3; and $[e_{\mathrm{ES}}]$ is the Voigt coupling matrix

TABLE 2: Typical physical parameters for the ultrasonic-solid-pMUT coupling simulation model [18, 19].

Components		Materials	Density (kg/m^3)	Young's modulus (GPa)	Poisson's ratio	Relative permittivity
Top and bottom electrodes		Pt	21450	168	0.38	1.0
Substrate		Si	2329	170	0.28	11.7
Piezoelectric layer	Emitter	PZT-4	7500	—	—	$[\varepsilon_{rS1}]$
	Receiver	PZT-5				$[\varepsilon_{rS2}]$
GIS enclosure		Al	2700	70	0.33	1.0

for anisotropic materials. In this study, the 6×6 elastic matrix $[c_E]$ and 3×6 coupling matrix $[e_{ES}]$ for anisotropic piezoelectric materials of PZT-4 and PZT-5 are presented in Table 3, respectively [18].

In the actual pMUT system, there exists the damping effect. Rayleigh damping is usually used to describe the mechanical loss caused by the system damping in the transient dynamic analysis. Since the damping ratio of pMUT structure is unknown at the design stage, a structured loss factor (η_s) is introduced to describe the mechanical loss, and the original elastic matrix is changed as follows:

$$[c_E] \longrightarrow (1 + i\eta_s)[c_E]. \tag{4}$$

For the top and bottom electrodes of pMUT, the charge conservation equation is formulated in equation (5), and the D-E constitutive relationship based on the dielectric model of relative permittivity is formulated in equation (6).

$$\begin{cases} \vec{E} = -\nabla V, \\ \nabla \cdot \vec{D} = \rho_v. \end{cases} \tag{5}$$

D-E constitutive relationship:

$$\vec{D} = \gamma_0 \gamma_r \vec{E}, \tag{6}$$

where V is the potential, v; γ_0 is the vacuum dielectric constant, $10^{-9}/36\pi$ F/m; and γ_r is the relative permittivity.

The propagation of ultrasonic waves in GIS enclosure is solved by using the transient pressure acoustic model, as formulated in equation (7), and the ultrasonic waves are coupled to the pMUT by using acoustic-structural boundary conditions, as formulated in equation (8) [21].

$$\frac{1}{\rho_c c^2} \frac{\partial^2 p_t}{\partial t^2} + \nabla \cdot \left(-\frac{1}{\rho_c} (\nabla p_t - \vec{q}_d) \right) = 0, \tag{7}$$

$$\begin{cases} -\vec{n} \cdot \left(-\frac{1}{\rho_c} (\nabla p_t - \vec{q}_d) \right) = -\vec{n} \cdot \vec{u}_{tt} \\ \vec{F}_A = p_t \vec{n} \end{cases}, \tag{8}$$

where ρ_c is the structure density, kg/m^3; p_t is the total sound pressure, Pa; c is the sound velocity, 6300 m/s; $\vec{q}_d$ is the dipole domain source; $\vec{n}$ is the surface normal; $\vec{u}_{tt}$ is the structural acceleration, m/s^2; and $\vec{F}_A$ is the load per unit area of the structure, N/m^2.

The boundary conditions are set as follows. For the emitting pMUT, voltage excitation is input on the top electrode surface and the bottom electrode is grounded, which are formulated in the following equation:

$$\begin{cases} V = V_0(t), \\ V = 0, \end{cases} \tag{9}$$

where V_0 is the input voltage excitation, V. In the present study, one cycle of signal excitation is considered, and the input voltage signal waveform is formed by combining the sine wave and rectangular wave, as shown in Figure 2 [18, 22]. The voltage signal amplitude is set to 50 V. In order to observe the transmission process of acoustic waves in the GIS enclosure and reduce the calculation amount of simulation work, the voltage excitation frequency is set to 20 MHz according to the initial pMUT structure size.

For the receiving pMUT, floating potential is set on the top electrode surface and the bottom electrode is grounded, which are formulated in the following equation:

$$\begin{cases} V \equiv \text{const}, \\ \int_{\partial\Omega} (\vec{D} \cdot \vec{n}) dA = 0, V = 0. \end{cases} \tag{10}$$

For structural mechanics boundary settings, the side boundaries of the pMUT substrate are set as fixed constraint and all other boundaries are free. The fixed constraint boundary is set as follows:

$$\vec{u} = 0. \tag{11}$$

In the present work, since only the process of receiving direct ultrasonic signals by receiving pMUT is considered, the hard sound field wall boundary setting is adopted on the surfaces, where the GIS enclosure and the pMUT are not directly contacted, which means the acoustic waves are completely reflected on these walls. The governing equation is as follows:

$$-\vec{n} \cdot \left(-\frac{1}{\rho_c} (\nabla p_t - \vec{q}_d) \right) = 0. \tag{12}$$

All the above equations are coupling solved based on the finite element software COMSOL Multiphysics. The MUMPS direct solver is used to solve the equations of pressure acoustics and solid mechanics, and the fluxes at the interface between different regions are kept equal. When solving the transient propagation process of ultrasonic, the time step is set as 1/5 of the vibration period, and the computation is considered to be convergent when the iterative calculation residual is less than 10^{-4}. For the characteristic frequency and frequency domain analysis of the pMUT, when the iterative calculation residual is less than 10^{-6}, the computation is considered to be convergent.

TABLE 3: Elastic and coupling matrices for piezoelectric layer materials [18].

Parameters		Symbols	PZT-4	PZT-5
$[c_E] = \begin{bmatrix} c_{11} & c_{12} & c_{13} & & & \\ c_{12} & c_{11} & c_{13} & & & \\ c_{13} & c_{13} & c_{33} & & & \\ & & & c_{44} & & \\ & & & & c_{44} & \\ & & & & & c_{66} \end{bmatrix} \times 10^{10}$ Pa		c_{11}	13.9	12.7
		c_{12}	7.78	8.02
		c_{13}	7.43	8.47
		c_{33}	11.5	11.7
		c_{44}	2.56	2.3
		c_{66}	3.06	2.35
$[e_{ES}] = \begin{bmatrix} & & & & e_{15} & \\ & & & e_{15} & & \\ e_{31} & e_{31} & e_{33} & & & \end{bmatrix}$ C/m^2		e_{15}	12.72	17.03
		e_{31}	−5.20	−6.62
		e_{33}	15.08	23.24
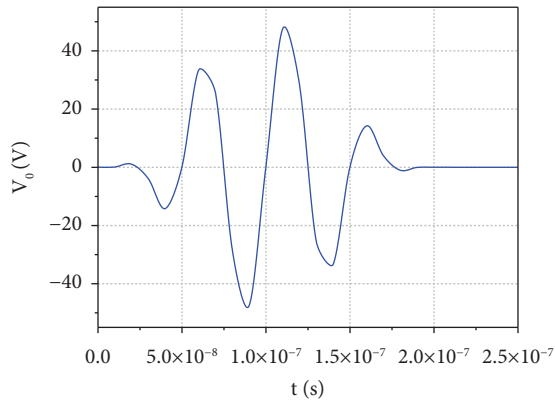
FIGURE 2: Input voltage excitation of emitting pMUT [18, 22].

FIGURE 3: Computational grids for the 2D acoustic-solid-pMUT coupling model and 3D pMUT model.

3. Grid Independence Test and Model Validations

3.1. Grid Independence Test. First, the grid independence test was performed. In this article, the computational grids for the two-dimensional acoustic-solid-pMUT coupling model and the three-dimensional pMUT model are presented in Figure 3. For the two-dimensional coupling model, an unstructured grid is constructed for the computation, the maximum grid size of the GIS enclosure domain (zone 2) is limited according to the ultrasonic wavelength, and the grid of the pMUT piezoelectric layer is locally refined. The input voltage excitation is shown in Figure 2. Five sets of grids are adopted for the simulation tests, and the specific grid settings and computational results are presented in Table 4. The results show that when the total grid number is increased from 26804 (grid 4) to 38426 (grid 5), the central displacement amplitude (u_{max}) and output voltage amplitude (V_{max}) of receiving pMUT only change by 1.09% and 0.53%, respectively. Therefore, grid 4 with total element number of 26804 should be good enough for the test, and the similar mesh settings to grid 4 is finally adopted for the subsequent acoustic-solid-pMUT coupling simulations. For the three-dimensional pMUT model, a structured grid is constructed for the substrate and bottom electrode (zone 4), while zone 5 and zone 6 are meshed with free tetrahedral grids. Five sets of grids are adopted for the simulation tests, and the specific grid settings and computational results are presented in Table 5. It shows that when the total grid number changes
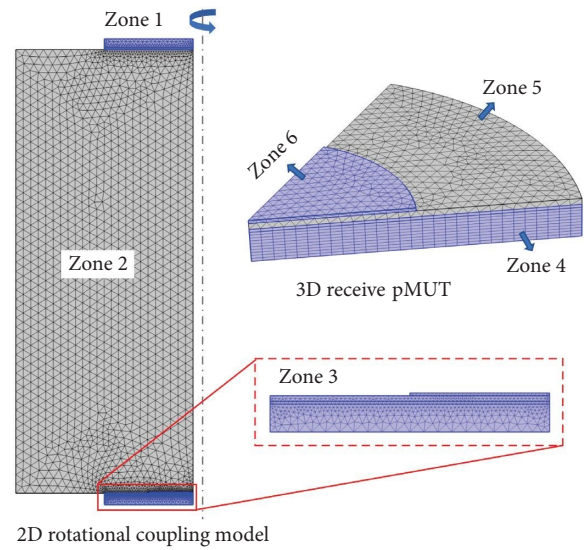
from 36669 (grid 3) to 55010 (grid 4), the inherent frequency (f_0) and effective electromechanical coupling factor (K_{eff}^2) of the receiving pMUT are almost unchanged. Therefore, grid 3 with total element number of 36669 should be good enough for the simulations, and similar mesh settings to grid 3 is adopted for the subsequent frequency analysis of pMUT.

3.2. Model Validations. In order to validate the computational model of pMUT, the performance of circular pMUT based on AlN film in [15] was restudied in this section. The physical model and geometric dimensions for the pMUT validation model are presented in Figure 4. It shows that the aluminum electrode is selected in the validation model, the piezoelectric layer is the AlN film, and the special substrate structure is adopted to improve the pMUT stability and its matching with air. Typical physical parameters of each component for the validation model are presented in Table 6. First, the inherent frequency of the pMUT is simulated and analyzed. The comparison between the simulation results in this article and the experimental results in [15] is presented in Table 7. The results show that the current simulation results are in good agreement with the experimental results [15], and the relative deviation of the inherent frequency is

TABLE 4: The central displacement amplitude ($u_{\max}$) and output voltage amplitude ($V_{\max}$) in acoustic-solid-pMUT coupling simulation for different computational grids.

Grids	Regions	Minimal grid size (μm)	Maximal grid size (μm)	Total grid numbers	$u_{\max} \times 10^{-3}$ (μm)	$V_{\max}$ (V)
Grid 1	Zone 1	19.27	142.86	5748	3.02	1.35
	Zone 2	10.01	176.77			
	Zone 3	7.59	124.09			
Grid 2	Zone 1	19.25	100.00	10717	2.62	1.74
	Zone 2	10.00	118.03			
	Zone 3	6.55	124.09			
Grid 3	Zone 1	18.11	76.92	17706	2.71	1.82
	Zone 2	10.00	92.25			
	Zone 3	6.25	111.62			
Grid 4	Zone 1	12.84	62.50	26804	2.75	1.87
	Zone 2	9.84	71.99			
	Zone 3	5.87	100.23			
Grid 5	Zone 1	11.12	52.63	38426	2.78	1.88
	Zone 2	9.26	61.24			
	Zone 3	5.57	60.18			

TABLE 5: The inherent frequency (f_0) and effective electromechanical coupling factor (K_{eff}^2) of receiving pMUT for different computational grids.

Grids	Regions	Minimal grid size (μm)	Maximal grid size (μm)	Total grid numbers	f_0 (kHz)	K_{eff}^2 (%)
Grid 1	Zone 4	142.49	264.34	8152	314	11.03
	Zone 5	25.79	264.34			
	Zone 6	32.41	83.62			
Grid 2	Zone 4	51.69	114.61	21253	312	10.96
	Zone 5	24.89	114.61			
	Zone 6	23.70	67.25			
Grid 3	Zone 4	44.32	100.81	36669	310	10.93
	Zone 5	19.00	100.81			
	Zone 6	20.84	51.43			
Grid 4	Zone 4	34.34	67.38	55010	310	10.92
	Zone 5	17.09	67.38			
	Zone 6	17.59	41.25			

only 0.5%. When 10 V alternating current is applied to the electrode, the piezoelectric layer (AlN) vibrates due to the inverse piezoelectric effect and generates acoustic waves, and then, the acoustic waves propagate in the air domain (when $T_{\mathrm{air}} = 293.15$ K, the acoustic velocity is 343.2 m/s). Liu et al. [15] measured the sound pressure level distribution at a height of 20 mm from the vibration plane. The comparison between the measurement results in [15] and the simulation results in this article is presented in Figure 5. It shows that the present computational results can agree well with the experimental results as reported in [15]. The maximum deviation of the sound pressure level at the same height is 4.31 dB and its relative deviation is 2.82%. Therefore, it is considered that the numerical models and computational methods adopted in this article are reasonable and reliable.

4. Results and Discussion

4.1. Acoustic-Solid-Electric Signal Conversion and pMUT Sensing Characteristics Analysis. First, the conversion process between ultrasonic and output electric signals is

simulated and analyzed. From the composite waveform of the electric signal (Figure 2), it should be noticed that the voltage excitation is input between 0 and 2×10^{-7} s. Then, the acoustic waves are generated due to the diaphragm deformation and vibration of emitting pMUT, and the acoustic pressure distributions in GIS enclosure at different moments are presented in Figure 6. It shows that the propagation speed of acoustic waves inside the GIS enclosure is fast, and the direct waves reach the receiving pMUT within 1 μs. The acoustic waves are diffused and transmitted in the form of spherical wave, and the amplitude of sound pressure at the vertical direction of emitting pMUT is maximum. Since the pressure direction of the direct wave is parallel to the polarization direction of the piezoelectric layer, the induced charges are generated in receiving the pMUT piezoelectric layer and electric signals are output through the electrode. The variations of the input and output electric signals obtained from acoustic-solid-pMUT coupling simulations are presented in Figure 7. The results show that the direct acoustic wave arrives at the receiving pMUT at about 8×10^{-7} s and the frequency of the simulated output electric
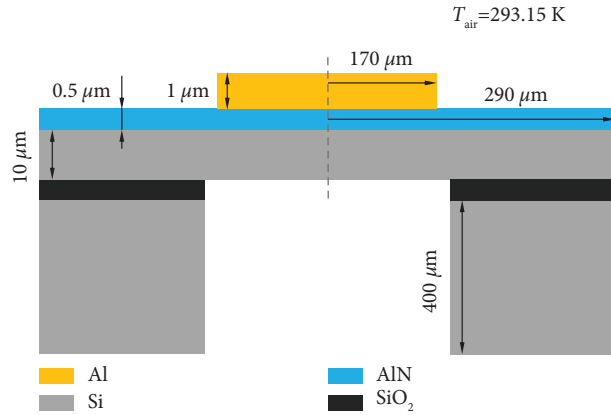
FIGURE 4: Physical model and geometric dimensions for the pMUT validation model [15].

TABLE 6: Typical physical properties of different components for the pMUT validation model [15].

Components	Materials	Density (kg/m^3)	Young's modulus (GPa)	Poisson's ratio	Relative permittivity
Electrode	Al	2700	70	0.33	1.0
Piezoelectric layer	AlN	3300	—	—	9.0
Substrate	Si	2329	170	0.28	11.7
	SiO$_2$	2200	70	0.17	4.2

TABLE 7: Comparison of the pMUT inherent frequency for present simulation and experiment results [15].

Parameter	Present simulation	Experiment [15]	Relative deviation (%)
Inherent frequency (kHz)	402	400	0.5
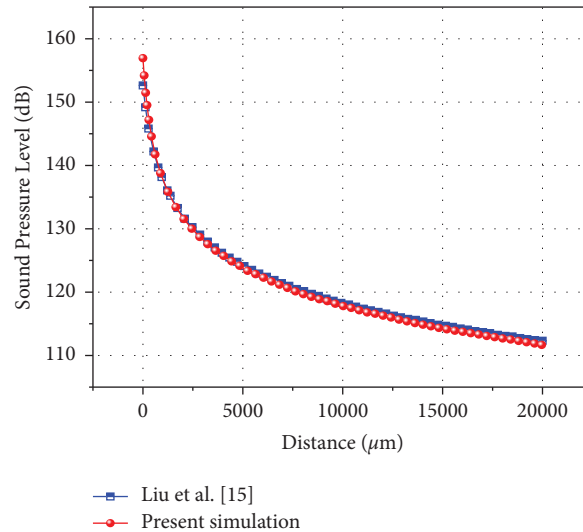
FIGURE 5: Comparison of the sound pressure level distribution for present simulation and experiment results [15].

signal is consistent with the input electric signal, while the amplitude of the output voltage (1.88 V) attenuates greatly as compared with the input voltage (50 V). This is mainly caused by the large deviation between the input excitation frequency (Figure 2), pMUT resonant frequency (see Table 8), and the low sensitivity of the sensor. In addition, since

there exist mechanical losses when the piezoelectric layer vibrates, the energy would be attenuated during acoustic waves transmission.

In the numerical study of emitting pMUT, most researchers have strictly modeled pMUTs containing electrode structures, while some researchers have simplified the
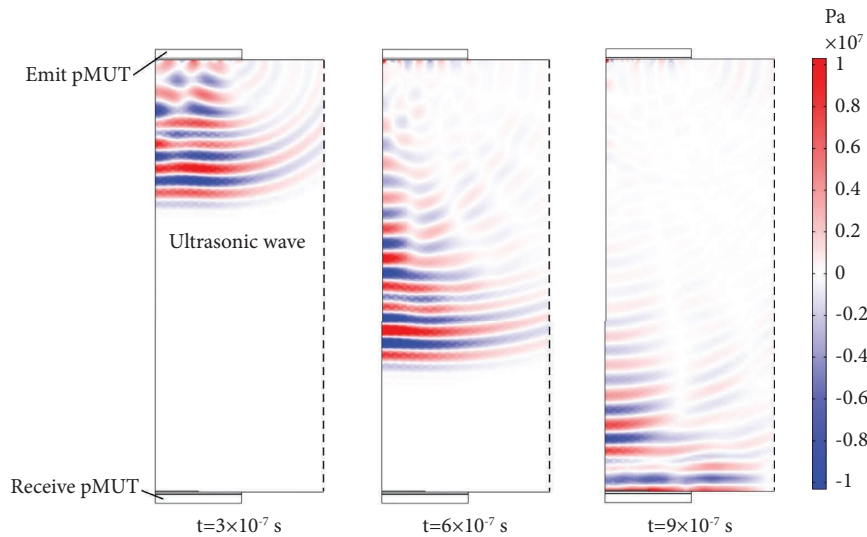
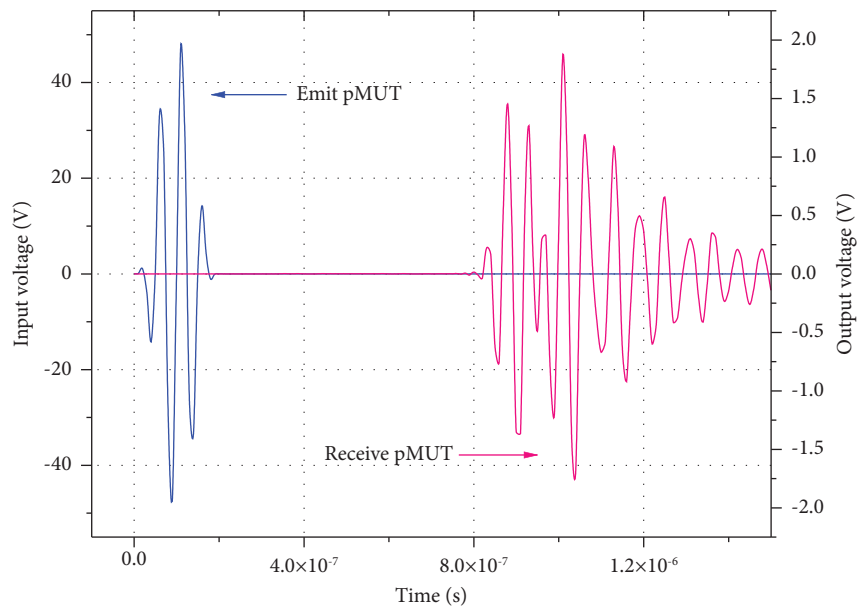FIGURE 6: Acoustic pressure distributions in GIS enclosure at different moments.

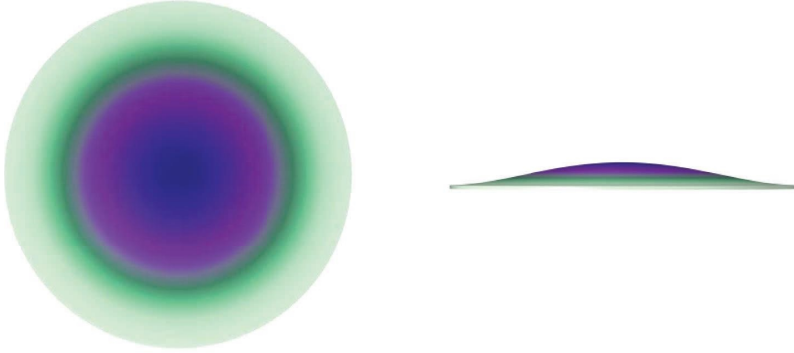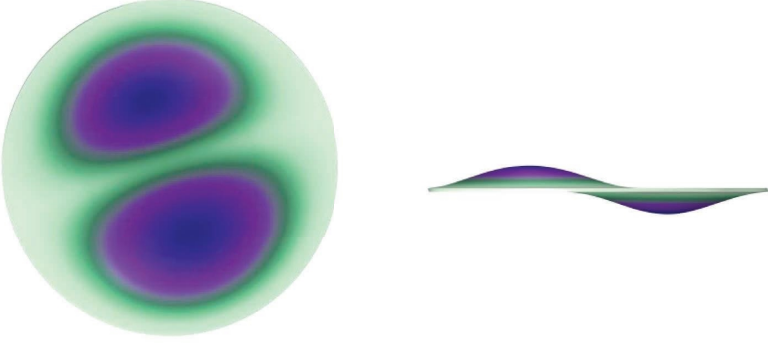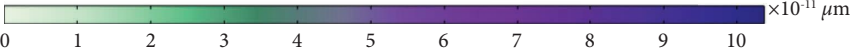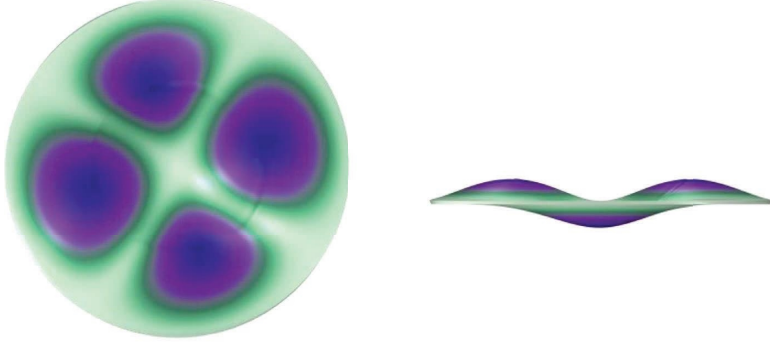FIGURE 7: Variations of the input and output electric signals of pMUT.

electrode structures (top or bottom electrodes) by setting boundary conditions [17, 23]. In this article, the effect of the top electrode on the acoustic-solid-electric coupling simulation of pMUT is further discussed. The simulation models of receiving pMUT with the unsimplified top electrode and simplified top electrode (using boundary conditions to replace the top electrode) are established, and the comparison of output electric signals for different models is presented in Figure 8. The results show that after simplifying the top electrode, the output response of the receiving pMUT is obviously weakened, the attenuation speed of the output electric signal increases, and the output voltage amplitude decreases to 1.35 V, which is 28.2% lower than that of model with the unsimplified top electrode (1.88 V). This is mainly because when the upper surface of the PZT is set as

the electrode boundary, it is equivalent to set the top electrode completely covered by the PZT membrane, and the energy loss is larger. In addition, due to top electrode simplification, the first-order inherent frequency of the receiving pMUT obtained from numerical simulation changes to 330 kHz, which is 6.45% higher than the actual value (310 kHz). Therefore, simplifying the top electrode will lead to relatively large errors when simulating the acoustic-solid-electric coupling transfer process of pMUT.

Then, the sensing response characteristics of pMUT are analyzed. The working frequency of the ultrasonic transducer is an important characteristic parameter. When pMUT acts as an acoustic receiver, the closer the vibration frequency of ultrasonic waves to the resonant frequency of membrane, the better response performance of the pMUT.

TABLE 8: The first-, second-, and third-order modal shapes and inherent frequencies of receiving pMUT.

Modes	Modal shape	Inherent frequency (kHz)
First		310
Second		645
Third		1042

In the current study, the first-, second-, and third-order modal shapes of receiving the pMUT piezoelectric layer are presented in Table 8, and their corresponding inherent frequencies are 310 kHz, 645 kHz, and 1042 kHz, respectively. The membrane has the maximum amplitude under the first mode, and the amplitude decreases with the increase of vibration mode order. In addition, the multipoint phase of the piezoelectric membrane is different under higher order modes, which is not conducive to the demodulation of ultrasonic signals. Therefore, controlling the first-order inherent frequency of the receiving pMUT within the optimal frequency range of the ultrasonic signal from GIS discharge can improve its detection sensitivity.

Besides, the effective electromechanical coupling coefficient (K_{eff}^2) is also an important performance parameter of pMUT, which reflects the coupling strength between mechanical and electrical energy through the piezoelectric effect as piezoelectric membrane vibrates. K_{eff}^2 can be expressed by the resonant frequency (f_r) and antiresonant frequency (f_a), as formulated in equation (13) [24]. When the pMUT piezoelectric membrane resonates, the impedance is minimum and the susceptance is maximum. When the
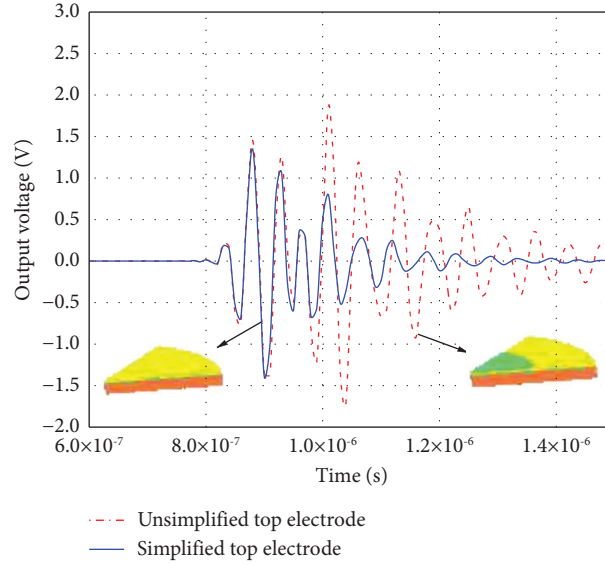
FIGURE 8: Comparison of output electric signals for unsimplified and simplified top electrode models.

excitation frequency reaches the antiresonant frequency of membrane, the impedance is maximum and the susceptance is minimum. In this study, the admittance distributions of receiving pMUT at different frequencies are presented in Figure 9. The results show that the resonant frequency of the pMUT is 302.2 kHz, the antiresonant frequency is 320.2 kHz, and the effective electromechanical coupling coefficient (K_{eff}^2) is 10.93%.

$$K_{\text{eff}}^2 = 1 - \left(\frac{f_r}{f_a}\right)^2. \tag{13}$$

4.2. Structural Optimization and Design of Receiving pMUT. Based on the abovementioned analysis, it could be known that reducing the difference between the resonant frequency of receiving pMUT and the ultrasonic excitation frequency and increasing the effective electromechanical coupling coefficient of the sensor can improve detection sensitivity for GIS discharge. The frequency of the ultrasonic signal generated by GIS breakdown discharge is generally between 20 kHz and 200 kHz, and more signals are concentrated around 80 kHz [25]. Therefore, this section aims to design a receiving pMUT with a resonant frequency around 80 kHz and a large effective electromechanical coupling coefficient, which would have good response characteristics when detecting GIS discharge. Since the actual damping of the system is unknown at the design stage and the deviation between the resonant and inherent frequencies is small, the inherent frequency is studied instead of the resonant frequency during the process of structural optimization.

The influence of piezoelectric layer radius (R), piezoelectric layer thickness (d), top electrode radius (R_0), and substrate thickness (d_{si}) on the inherent frequency (f_0) and the effective electromechanical coupling coefficient (K_{eff}^2) of receiving pMUT are analyzed through finite element

simulations, and a relatively optimal pMUT structure is proposed for GIS discharge detection. First, the inherent frequencies and effective electromechanical coupling coefficients under different top electrode radii and different piezoelectric layer radii are calculated ($d_{\text{si}} = 100\,\mu\text{m}$ and $d = 40\,\mu\text{m}$), as presented in Figures 10(a) and 10(b), respectively. The results show that the effect of the piezoelectric layer radius (R) on the inherent frequency (f_0) of pMUT is remarkable. With the increase of the membrane and substrate area, the inherent frequency of pMUT decreases gradually. When the piezoelectric layer radius (R) is 2000 μm, the inherent frequency of pMUT is around 80 kHz. The impact of the coverage area of the top electrode ($\pi R_0{}^2$) on the inherent frequency (f_0) is relatively small, while its impact on the effective electromechanical coupling coefficient (K_{eff}^2) is relatively large. When the coverage area ratio of the top electrode is between 30% and 80%, the K_{eff}^2 is high and has a maximum value. When the piezoelectric layer radius (R) is 2000 μm and the top electrode radius (R_0) is 1000 μm, the K_{eff}^2 is maximum.

Since increasing piezoelectric layer thickness (d) will decrease center static displacement of pMUT, in this study, the relationship between receiving sensitivity and piezoelectric layer thickness (d) of receiving pMUT is analyzed to determine the range of piezoelectric layer thickness (d). The receiving sensitivity is represented by the ratio of the voltage at the output of pMUT to the input sound pressure at center of transducer receiving surface, and its relationship with piezoelectric layer thickness (d) is presented in Figure 11. It shows that when the piezoelectric layer thickness (d) is larger than 100 μm, the receiving sensitivity almost does not increase with the piezoelectric layer thickness (d). Therefore, in this study, only $d \leq 100\,\mu\text{m}$ is considered. Then, the substrate thickness (d_{si}) and piezoelectric layer thickness (d) are determined. When $R = 2000\,\mu\text{m}$ and $R_0 = 1000\,\mu\text{m}$, the variations of the inherent frequency (f_0) for pMUT under
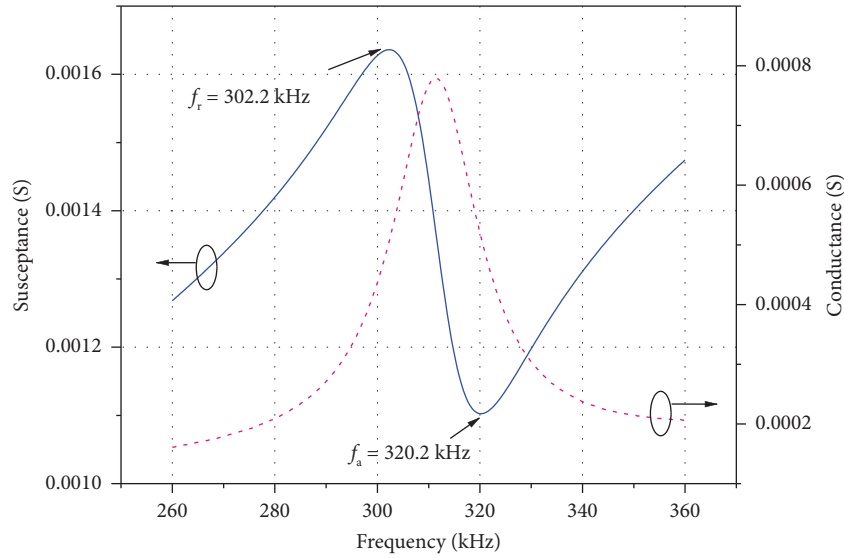
Figure 9: Admittance distributions of receiving pMUT at different frequencies.
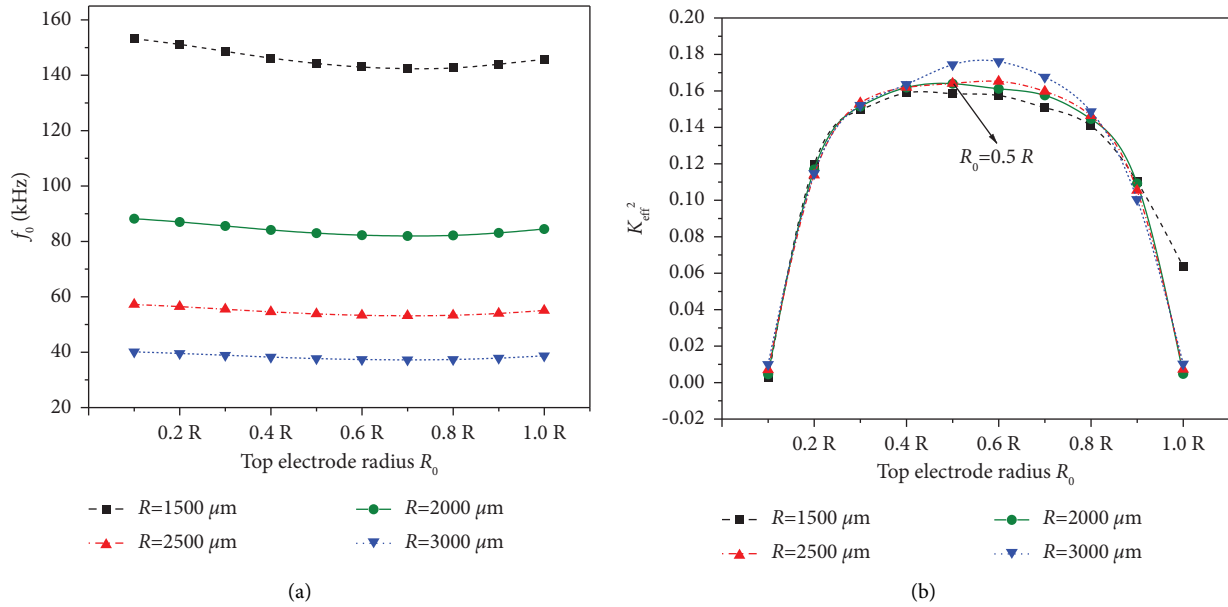

(a)

(b)

Figure 10: Variations of the inherent frequency and the effective electromechanical coupling coefficient under different top electrode radii and piezoelectric layer radii ($d_{si} = 100 \, \mu m$ and $d = 40 \, \mu m$). (a) Variations of the inherent frequency (f_0). (b) Variations of the effective electromechanical coupling coefficient (K_{eff}^2).

different piezoelectric layer thickness (d) and substrate thickness (d_{si}) are presented in Figure 12. It shows that the inherent frequency (f_0) almost increases linearly with the substrate thickness (d_{si}), and only when $d_{si} \geq 80 \, \mu m$, the inherent frequency reaches 80 kHz. Therefore, the receiving pMUT structure should be determined based on the substrate thickness (d_{si}) of $80 \, \mu m$, $90 \, \mu m$, and $100 \, \mu m$.

Figure 13(a) shows that the inherent frequency (f_0) of pMUT is proportional to the piezoelectric layer thickness (d), and the f_0 is around 80 kHz when the substrate thickness (d_{si}) is $80 \, \mu m$, $90 \, \mu m$, and $100 \, \mu m$ with corresponding piezoelectric layer thickness (d) of $100 \, \mu m$, $60 \, \mu m$, and $20 \, \mu m$, respectively. Figure 13(b) shows that the effective

electromechanical coupling coefficient (K_{eff}^2) of pMUT increases with piezoelectric layer thickness (d) and its increasing rate decreases gradually. When the substrate thickness (d_{si}) is $80 \, \mu m$ and piezoelectric layer thickness (d) is $100 \, \mu m$, the effective electromechanical coupling coefficient (K_{eff}^2) is maximum, which is 22.59%. Therefore, when the piezoelectric layer radius (R) is $2000 \, \mu m$, top electrode radius (R_0) is $1000 \, \mu m$, piezoelectric layer thickness (d) is $100 \, \mu m$, and substrate thickness (d_{si}) is $80 \, \mu m$, and the receiving pMUT structure should be optimum. For this case, the inherent frequency (f_0) of receiving pMUT is 80.16 kHz, which is suitable for ultrasonic signal detection of GIS breakdown discharge, and the effective
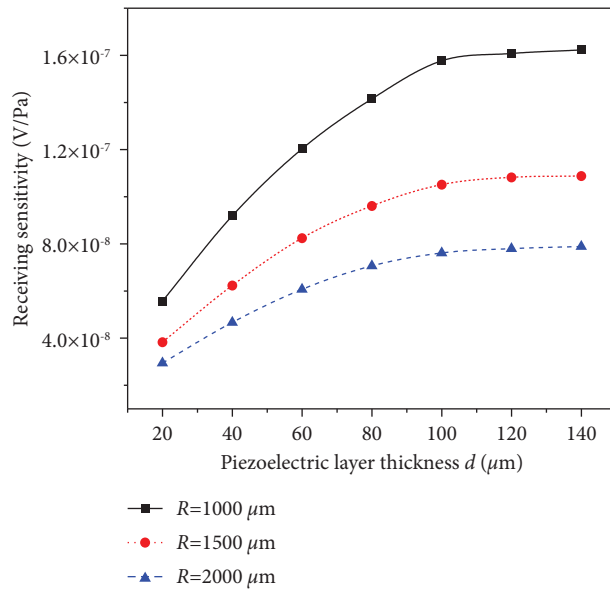
Figure 11: Variations of receiving sensitivity of pMUT under different piezoelectric layer thickness.
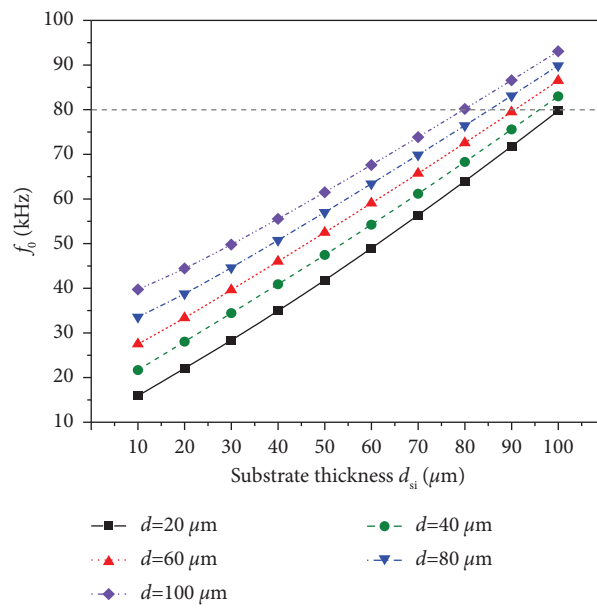

Figure 12: Variations of the inherent frequency of pMUT under different substrate thickness and piezoelectric layer thickness ($R = 2000\,\mu$m, $R_0 = 1000\,\mu$m).
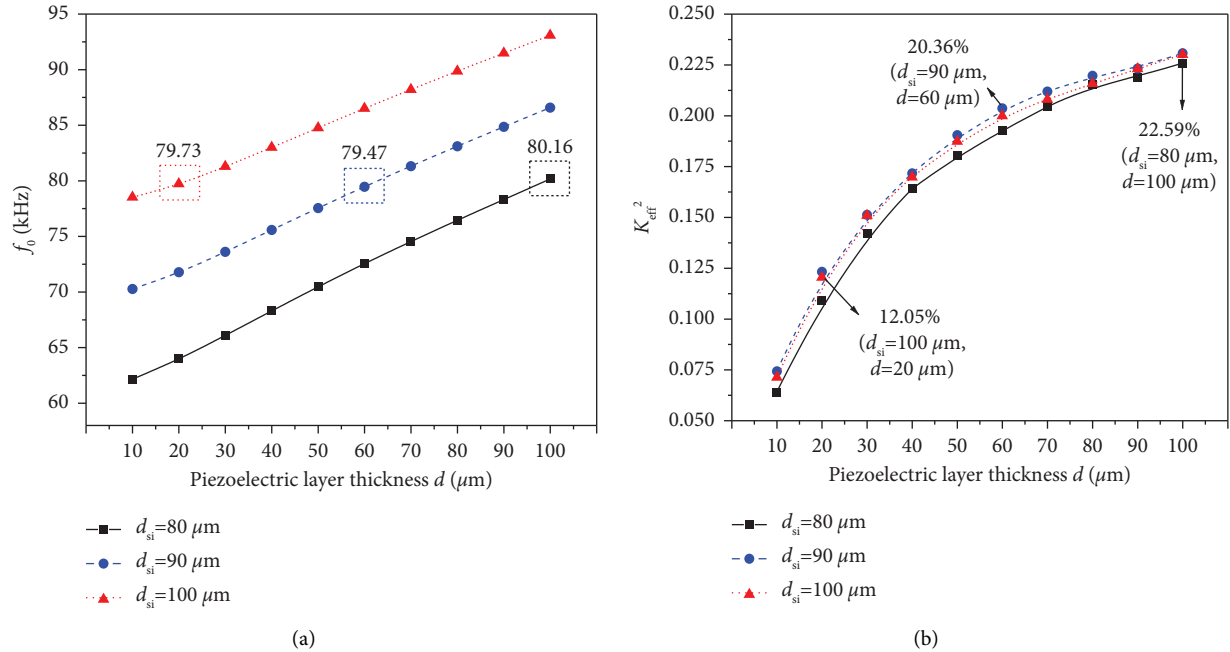
FIGURE 13: Variations of inherent frequencies and effective electromechanical coupling coefficients under different piezoelectric layer thickness ($R = 2000\,\mu$m and $R_0 = 1000\,\mu$m). (a) Variations of the inherent frequency (f_0). (b) Variations of the effective electromechanical coupling coefficient (K_{eff}^2).

electromechanical coupling coefficient (K_{eff}^2) is 22.59%, which is 106.7% higher than the result before structural optimization ($K_{\text{eff}}^2 = 10.93$%).

5. Conclusions

In the present article, the ultrasonic-solid-pMUT coupling simulation model was established to investigate the propagation process of ultrasonic waves in GIS enclosure and the conversion between ultrasonic and electric signals through pMUT. The output electric signals for the unsimplified top electrode and simplified top electrode model were compared, and the structure of receiving pMUT was optimized according to the main ultrasonic frequency range of GIS breakdown discharge and the key performance parameters of pMUT. The major findings are as follows:

(1) In the present ultrasonic-solid-pMUT coupling simulations, the frequency of the simulated output electric signal is consistent with the input electric signal, while the amplitude of the output voltage (1.88 V) attenuates greatly as compared with the input voltage (50 V). During numerical simulations, simplifying the top electrode will lead to relatively large errors. The output response of simplified pMUT is obviously weakened, the attenuation rate of the output electric signal increases, and the output voltage amplitude further decreases. Furthermore, simplifying top electrode will also lead to a higher inherent frequency of pMUT as compared with the actual value.

(2) Both the effects of piezoelectric layer radius (R) and substrate thickness (d_{si}) on the inherent frequency (f_0) of pMUT are remarkable. The f_0 is inversely proportional to R, while directly proportional to d_{si}. When the coverage area ratio of the top electrode is between 30% and 80%, the effective electromechanical coupling coefficient (K_{eff}^2) is high and has a maximum value. When the piezoelectric layer thickness (d) is larger than $100\,\mu$m, the receiving sensitivity nearly does not increase with the piezoelectric layer thickness. For the optimum pMUT structure, the inherent frequency (f_0) of receiving pMUT is 80.16 kHz, which is suitable for ultrasonic signal detection of GIS breakdown discharge, and the effective electromechanical coupling coefficient (K_{eff}^2) is 22.59%, which is 106.7% higher than the result before structural optimization ($K_{\text{eff}}^2 = 10.93$%).

Nomenclature

A:	Surface area (m^2)
c:	Sound velocity (m/s)
c_E:	Elastic matrix
$\vec{D}$:	Electric displacement (C/m^2)
d:	Piezoelectric layer thickness (μm)
d_{pt}:	Electrode th3ickness (μm)
d_{si}:	Substrate thickness (μm)
$\vec{E}$:	Electric field strength (N/C)
e_{ES}:	Coupling matrix
e^T:	Piezoelectric stress constant

$\vec{F}_A$:   Load per unit area of the structure (N/m^2)
f_0:   Inherent frequency (Hz)
f_a: Antiresonant frequency (Hz)
f_r: Resonant frequency (Hz)
K_{eff}^2:   Effective electromechanical coupling coefficient
$\vec{n}$:   Surface normal
p_t: Total sound pressure (Pa)
$\vec{q}_d$:   Dipole domain source
R: Piezoelectric layer or substrate radius (μm)
R_0:   Top electrode radius (μm)
S: Stress (Pa)
T_{air}:   Ambient air temperature (K)
t: Time (s)
$\vec{u}$:   Structural displacement vector (m)
$\vec{u}_{\text{tt}}$:   Structural acceleration (m/s^2)
V: Potential (v)

Greek letters

γ_0:   Vacuum dielectric constant (F/m)
γ_r: Relative permittivity
ε: Strain
ε_0:   Initial prestrain
ε_{rS}:   Relative permittivity
η_s: Structured loss factor
ρ: Density (kg/m^3).
ρ_v: Volume electric charge density (C/m^3).

Data Availability

The data used to support the findings of this study are included within the article.

Conflicts of Interest

The authors declare that they have no conflicts of interest.

Acknowledgments

References

[1] F. Atalar, E. Dokur, E. Balaban, M. Missous, and M. Ugur, "Partial discharge detection in pressboards immersed in mineral insulation oil with quantum well hall effect magnetic field sensors," *IEEE Access*, vol. 10, pp. 70362–70369, 2022.

[2] F. Atalar, A. Ersoy, and P. Rozga, "Investigation of effects of different high voltage types on dielectric strength of insulating liquids," *Energies*, vol. 15, no. 21, p. 8116, 2022.

[3] F. Atalar, C. P. Uzunoglu, S. Cekli, and M. Ugur, "Statistical analysis of induced magnetic fields on oil-impregnated insulation pressboards," *Electrical Engineering*, vol. 102, no. 4, pp. 2095–2107, 2020.

[4] H. L. Lin, Z. Y. Zhang, H. S. Liu, Y. F. Wang, Y. N. Liu, and D. Y. Yu, "Interference to the secondary cable caused by a very fast transient overvoltage in a gas-insulated switchgear substation," *Mathematical Problems in Engineering*, vol. 2022, Article ID 5396788, 10 pages, 2022.

[5] R. Jia, Y. T. Xie, H. Wu, J. Dang, and K. S. Dong, "Power transformer partial discharge fault diagnosis based on multidimensional feature region," *Mathematical Problems in Engineering*, vol. 2016, Article ID 4835694, 11 pages, 2016.

[6] C. Wei, J. Xiong, and S. Yang, "Analysis and field application of live detection of partial GIS discharge," *Electrical Automation*, vol. 38, no. 2, pp. 106–108+114, 2016.

[7] T. Li, F. Xue, and D. L. Wei, "Analysis and treatment of a free particle discharge defect in GIS," *Electrotechnics Electric*, vol. 272, no. 8, pp. 37–42, 2020.

[8] Z. H. He, Z. B. Yang, L. L. Xiao, Z. F. Huang, W. X. Si, and S. Q. Liu, "Design and application of wireless location system for GIS withstand voltage breakdown fault," *High Voltage Apparatus*, vol. 57, no. 1, pp. 41–47+54, 2021.

[9] J. Ling, Y. Q. Chen, Y. Chen et al., "Design and characterization of high-density ultrasonic transducer array," *IEEE Sensors Journal*, vol. 18, no. 6, pp. 2285–2290, 2018.

[10] U. H. Lim, J. H. Yoo, V. Kondalkar, and K. Lee, "Development of high frequency pMUT based on sputtered PZT," *Journal of Electrical Engineering & Technology*, vol. 13, no. 6, pp. 2434–2440, 2018.

[11] S. Pala and L. W. Lin, "An improved lumped element model for circular-shape pMUTs," *IEEE Open Journal of Ultrasonics, Ferroelectrics, and Frequency Control*, vol. 2, pp. 83–95, 2022.

[12] W. J. Liu, L. M. He, X. B. Wang et al., "3D FEM analysis of high-frequencyAlN-based PMUT arrays on cavity SOI," *Sensors*, vol. 19, no. 20, p. 4450, 2019.

[13] L. Wang, W. Zhu, Z. P. Wu, W. J. Liu, and C. L. Sun, "A novel coupled piezoelectric micromachined ultrasonic transducer based on piston mode," *IEEE Transactions on Ultrasonics, Ferroelectrics, and Frequency Control*, vol. 68, no. 11, pp. 3396–3405, 2021.

[14] G. Massimino, A. Colombo, L. D'Alessandro et al., "Multiphysics modelling and experimental validation of an aircoupled array of PMUTs with residual stresses," *Journal of Micromechanics and Microengineering*, vol. 28, no. 5, p. 9, Article ID 054005, 2018.

[15] X. X. Liu, X. Y. Chen, X. H. Le, Z. G. Xu, C. J. Wu, and J. Xie, "A high-performance square pMUT for rangefinder," in *Proceedings of the 13th Annual IEEE International Conference on Nano/Micro Engineered and Molecular Systems*, pp. 106–109, IEEE-NEMS, Singapore, April 2018.

[16] Z. Q. Xing, W. L. Ji, X. Y. Sun et al., "Design, characterization, and analysis of PZT micromachined piezoelectric ultrasonic transducers with good coupling to solids," *IEEE Transactions on Ultrasonics, Ferroelectrics, and Frequency Control*, vol. 67, no. 10, pp. 2135–2141, 2020.

[17] F. Sammoura, K. Smyth, and S. G. Kim, "An equivalent network representation of a clamped bimorph piezoelectric micromachined ultrasonic transducer with circular and annular electrodes using matrix manipulation techniques," *IEEE Transactions on Ultrasonics, Ferroelectrics, and Frequency Control*, vol. 60, no. 9, pp. 1989–2003, 2013.

[18] V. Comsol Multiphysics®, *5.2. Cn.comsol.com*, COMSOL AB, Stockholm, Sweden, 2016.

[19] C. H. Sun, Q. F. Shi, M. S. Yazici, T. Kobayashi, Y. F. Liu, and C. K. Lee, "Investigation of broadband characteristics of multi-frequency piezoelectric micromachined ultrasonic transducer (MF-pMUT)," *IEEE Sensors Journal*, vol. 19, no. 3, pp. 860–867, 2019.

[20] G. Massimino, F. Quaglia, A. Corigliano, and A. Frangi, "Model order reduction for the analysis of large arrays of

piezoelectric micromachined ultrasonic transducers in water," *Applied Acoustics*, vol. 182, p. 14, Article ID 108231, 2021.

[21] S. N. Meitei, K. Borah, and S. Chatterjee, "FEM based 3D modelling of partial discharge detection and localization in an oil-filled power transformer using piezoelectric acoustic sensor," *Tm-Technisches Messen*, vol. 87, no. 9, pp. 586–596, 2020.

[22] D. D. Zheng, S. H. Lv, and Y. Mao, "Effect mechanism of non-ideal flow field on acoustic field in gas ultrasonic flowmeter," *IET Science, Measurement & Technology*, vol. 13, no. 4, pp. 469–477, 2019.

[23] X. Kuan, R. M. Zhang, L. L. Zhang, and S. S. Zhou, "Free vibration analysis of bilayered piezoelectric circular plate based on the structure of PMUT," *Journal of Qilu university of technology*, vol. 35, no. 4, pp. 66–73, 2021.

[24] W. L. Wang, Y. Chiu, and D. Gong, "Effect of shared cavity on electromechanical performance of piezoelectric based micromachined ultrasonic transducer array," in *Proceedings of the 14th Annual IEEE International Conference on Nano/Micro Engineered and Molecular Systems (IEEE-NEMS)*, pp. 482–487, Bangkok, Thailand, April 2019.

[25] J. Y. Xue, M. X. Zhu, X. J. Shao, Y. B. Wang, J. B. Deng, and G. J. Zhang, "Simulation on ultrasonic propagation characteristics of partial discharge in ultra-high voltage GIS," *High Voltage Apparatus*, vol. 54, no. 9, pp. 67–75, 2018.